

Formation drivers and photochemical effects of ClNO₂ in a coastal city of Southeast China

Gaojie Chen^{1,4,5}, Xiaolong Fan^{1,4}, Haichao Wang^{2*}, Yee Jun Tham³, Ziyi Lin^{1,4,5}, Xiaoting Ji^{1,4,5}, Lingling Xu^{1,4}, Baoye Hu⁶, Jinsheng Chen^{1,4*}

¹Center for Excellence in Regional Atmospheric Environment, Institute of Urban Environment, Chinese Academy of Sciences, Xiamen 361021, China

²School of Atmospheric Sciences, Sun Yat-sen University, Zhuhai 519082, China

³School of Marine Sciences, Sun Yat-sen University, Zhuhai 519082, China

⁴Fujian Key Laboratory of Atmospheric Ozone Pollution Prevention, Institute of Urban Environment, Chinese Academy of Sciences, Xiamen 361021, China

⁵University of Chinese Academy of Sciences, Beijing 100049, China

⁶Minnan Normal University, Zhangzhou 363000, China

*Correspondence to: Jinsheng Chen (jschen@iue.ac.cn); Haichao Wang (wanghch27@mail.sysu.edu.cn).

Abstract. Nitryl chloride (ClNO₂) is an important precursor of chlorine (Cl) radical, significantly affecting ozone (O₃) formation and photochemical oxidation. However, the key drivers of ClNO₂ production are not fully understood. In this study, the field observations of ClNO₂ and related parameters were conducted in a coastal city of Southeast China during the autumn of 2022, combining with machine learning and model simulations to elucidate its key influencing factors and atmospheric impacts. Elevated concentrations of ClNO₂ (> 500 ppt) were notably observed during nighttime in late autumn, accompanied by increased levels of dinitrogen pentoxide (N₂O₅) and nitrate (NO₃⁻). Nighttime concentrations of ClNO₂ peaked at 3.4 ppb, while its daytime levels remained significant, reaching up to 100 ppt and sustaining at approximately 40 ppt at noon. Machine learning and field observations identified nighttime N₂O₅ heterogeneous uptake as the predominant pathway for ClNO₂ production, whereas NO₃⁻ photolysis contributed to its daytime generation. Additionally, ambient temperature (T) and relative humidity (RH) emerged as primary meteorological factors affecting ClNO₂ formation, mainly through their effects on thermal equilibrium and N₂O₅ hydrolysis processes, respectively. Ultraviolet (UV) radiation was found to play a dual role in ClNO₂ concentrations around noon. Box model simulations showed that under high ClNO₂ conditions, the rates of alkane oxidation by Cl radical in the early morning exceeded those by OH radical. Consequently, VOC oxidation by Cl radical contributed ~ 19% to RO_x production rates, thereby significantly impacting O₃ formation and atmospheric oxidation capacity. This research enriched the understanding of ClNO₂ generation and loss pathways, providing valuable insights for the regulation of photochemical pollution in coastal regions.

1 Introduction

Chlorine (Cl) radical, as an important atmospheric oxidant, can react with volatile organic compounds (VOCs) to affect RO_x (including OH, HO₂, and RO₂) radicals and ozone (O₃) formation (Yi et al., 2023), thereby perturbing atmospheric chemical components and air quality (Peng et al., 2021; Li et al., 2020). The reaction rates between Cl radical and some alkanes are several orders of magnitude faster than those involving OH radical (Atkinson et al., 2006). Furthermore, the related studies indicated that the production rates of Cl radical in the early morning could significantly exceed the production rates of OH radical formed via O₃ photolysis (Phillips et al., 2012; Tham et al., 2016), thereby enhancing the atmospheric oxidation capacity.

Nitryl chloride (ClNO₂) is one of the major Cl radical precursors in the tropospheric atmosphere (Thornton et al., 2010; Xue et al., 2015; Liu et al., 2017). It is mainly generated by the heterogeneous uptake of dinitrogen pentoxide (N₂O₅) on chloride-containing aerosols (Finlayson-Pitts et al., 1989; Thornton et al., 2010), among which N₂O₅ is produced through the equilibrium reaction with nitrogen dioxide (NO₂) and nitrate (NO₃) radical. Since Osthoff et al. (2008) firstly detected over 1 ppb of ClNO₂ in the urban outflows of America (Osthoff et al., 2008), significant production of ClNO₂ has been widely observed in the polluted coastal and inland areas with abundant anthropogenic emissions and chloride sources, with concentrations ranging from tens of ppt to several ppb (Riedel et al., 2012; Mielke et al., 2013; Mielke et al., 2011; Phillips et al., 2012; Bannan et al., 2015; Wang et al., 2016; Xia et al., 2020; Xia et al., 2021; Yun et al., 2018a; Wang et al., 2022; Li et al., 2023). For the diurnal profile of ClNO₂, its concentrations generally peaked and accumulated at midnight, then rapidly decreased to low levels due to strong photolysis after sunrise (Ma et al., 2023; Mielke et al., 2011; Xia et al., 2020). However, elevated daytime concentrations of ClNO₂ have been observed in field studies, mainly attributed to reduced photolysis rates under heavy cloud or fog cover, as well as contributions from horizontal and vertical transport (Tham et al., 2016; Xia et al., 2021; Jeong et al., 2019; Mielke et al., 2013; Bannan et al., 2015). Notably, the recent laboratory research demonstrated that nitrate (NO₃⁻) photolysis can generate ClNO₂ alongside Cl₂ (Dalton et al., 2023), yet this mechanism has not been confirmed under real atmospheric conditions.

At present, the observation studies of ClNO₂ focused on investigating its influencing factors, such as the N₂O₅ uptake coefficient and the production yield of ClNO₂ (Thornton et al., 2003; Tham et al., 2018). The field and laboratory studies have indicated that ClNO₂ production was mainly affected by ambient temperature (T), relative humidity (RH), and particle components (e.g., chloride (Cl⁻), NO₃⁻, and liquid water content) (Bertram and Thornton, 2009; Wang et al., 2023; Wang et al., 2020). In addition to

influencing factors, the photochemical effects of ClNO₂ photolysis have been extensively evaluated (Xue et al., 2015; Xia et al., 2021; Tham et al., 2016). Cl radical released by ClNO₂ photolysis will oxidize VOCs to promote the formation RO₂ radical and O₃, greatly compensating for the underestimation of RO₂ radical and O₃ generation in model simulations (Peng et al., 2021; Ma et al., 2023). The field measurements of ClNO₂ have been conducted in different atmospheric environments, while the key drivers of ClNO₂ chemistry were still not well recognized. Moreover, it is pertinent to explore whether there are additional and unrecognized sources of ClNO₂ beyond its heterogeneous generation from N₂O₅.

In this study, the comprehensive measurements of ClNO₂ and related parameters were conducted in a coastal city of Southeast China during the autumn of 2022. Field observations, combined with a machine learning model, were used to reveal the key driving factors of ClNO₂ formation. Furthermore, we further investigated the potential mechanisms driving daytime ClNO₂ generation. Additionally, we also assessed the photochemical impacts of ClNO₂ based on a box model. Overall, this study underscored the important role of NO₃⁻ in the ClNO₂ chemistry.

2 Materials and methods

2.1 Field Measurements

The intensive field measurements of ClNO₂, related precursors, and meteorological parameters from October 9th to December 5th, 2022 were performed at an urban site (Institute of Urban Environment, Chinese Academy of Sciences) in a coastal city (Xiamen) of Southeast China (Fig. S1). Here, ClNO₂, N₂O₅, gaseous pollutants (volatile organic compounds (VOCs), NO_x, SO₂, CO, and O₃), aerosol mass concentrations, ionic components, size distribution, and meteorological factors were simultaneously detected. Meanwhile, an iodide-adduct time-of-flight chemical ionization mass spectrometer (I⁻-ToF-CIMS) was used to measure ClNO₂ and N₂O₅. The principles and settings of I⁻-ToF-CIMS were similar with previous studies (Ma et al., 2023; Yan et al., 2023). Detailed descriptions of this observation site and instruments have been provided in previous work (Chen et al., 2024; Hu et al., 2022), Text S1, and Table S1. For the calibrations of ClNO₂ and N₂O₅, ClNO₂ was produced by passing Cl₂ (6 ppm in N₂) through a moist mixture of sodium nitrite (NaNO₂) and sodium chloride (NaCl) (Thaler et al., 2011; Wang et al., 2022), and N₂O₅ was synthesized by the reactions of O₃ and excessive NO₂ (Tham et al., 2016; Wang et al., 2016). The dependences of ClNO₂ and N₂O₅ sensitivities on relative humidity are presented in Fig. S2. The uncertainties of the ClNO₂ and N₂O₅ measurements were estimated to be ~20 %. The details of ClNO₂ and N₂O₅ calibrations and uncertainty analysis are displayed in Text S2.

2.2 Machine Learning model

Here, the extreme gradient boosting (XGBoost) model coupling with the Shapely additive explanations (SHAP) model (the XGBoost-SHAP model) was used to identify the key influencing factors of ClNO₂ formation. Meanwhile, the XGBoost model was applied to establish the predictive model of ClNO₂ based on the observed data of gaseous precursors and meteorological factors; the SHAP model was employed to evaluate the importance of each feature affecting the simulated concentrations of ClNO₂. The SHAP model is an interpretability tool designed to analyze the contributions of individual features to model predictions. It employs an additive explanatory framework that considers all features as contributors, drawing inspiration from cooperative game theory. For each predicted instance, SHAP assigns a Shapley value, representing the cumulative contribution of each feature. Positive SHAP values indicate that a feature increases the model's predicted outcome, signifying a positive contribution. Conversely, negative SHAP values suggest that the feature reduces the predicted value, reflecting a negative contribution. The absolute value of the SHAP score reflects the magnitude of the contribution, regardless of direction, offering insight into the overall importance of the feature. The true value, on the other hand, reveals the direction of the contribution (positive or negative), facilitating a clearer understanding of the relationship between the feature and the prediction. Besides, the partial dependence plot (PDP) analysis offers a visual representation of the marginal effect that the factors have on the model's predicted outcome. It is based on the principle of stabilizing the values of non-target features, and systematically altered the target feature's values according to the model's algorithmic framework to derive the predicted values.

ClNO₂ concentrations served as the dependent variable, with trace gases (SO₂, CO, NO₂, NO, O₃, and N₂O₅), PM_{2.5} and its inorganic compositions (NO₃⁻, SO₄²⁻, NH₄⁺, and Cl⁻), and meteorological parameters (T, RH, UV, WS, WD, and BLH) acting as independent variables. The simulated ClNO₂ concentrations by the XGBoost model were highly similar with the observed values ($R^2=0.91$), indicating the good performance of the XGBoost model (Fig. S3). Detailed introductions and settings of the XGBoost-SHAP model are provided in Text S3.

2.3 The box model

The observation-based model (OBM) was utilized to assess the impacts of ClNO₂ on photochemically atmospheric oxidation. As delineated in earlier studies (Xue et al., 2015; Tham et al., 2016; Xia et al., 2021; Peng et al., 2021; Peng et al., 2022), the Master Chemical Mechanism (MCM, version 3.3.1) was adopted, and established chlorine chemistry mechanisms have been integrated. The Tropospheric Ultraviolet and Visible Radiation (TUV) model was used to calculate ClNO₂ photolysis rates (J_{ClNO_2}) under clear-sky

conditions. The simulated $J\text{ClNO}_2$ values were then scaled based on field-measured $J\text{NO}_2$ values. A thorough exposition of the box model configuration can be found in our previous publications (Liu et al., 2022b; Liu et al., 2022a) and Text S4. Observation data, including ClNO_2 , VOCs, HCHO, HONO, CO, O_3 , NO, NO_2 , SO_2 , along with meteorological factors as constraint were input into the box model at an hourly resolution (Table S2). Due to the levels of ClNO_2 in the box model determined by observed levels of ClNO_2 , the parametrization for N_2O_5 uptake and ClNO_2 yield was not utilized in the box model. Two scenarios were examined: one representing observation-average conditions from October 9th to December 5th, the other reflecting a high ClNO_2 case observed on November 28th.

This study focused on elucidating the influence of ClNO_2 on the formation of RO_x radical and O_3 . The O_3 production rate minus the O_3 loss rate was used to calculate the net O_3 production rate (Eq. S1-3). The AOC is calculated by the sum of the rates of CH_4 , CO, and VOCs oxidized by atmospheric oxidants (O_3 , OH, Cl, and NO_3 radical) (Eq. S4) (Xue et al., 2015; Yi et al., 2023). Both scenarios were evaluated with and without including ClNO_2 inputs to assess its impacts on these processes.

3 Results and discussion

3.1 Overview of observations

Fig. 1 displays the time series of ClNO_2 , N_2O_5 , and related parameters including O_3 , NO_x , $\text{PM}_{2.5}$, Cl^- , NO_3^- , and meteorological parameters during the autumn observation period. Our observation shows a decline in T and UV values from October to November, with average RH values increasing from ~ 60% in October to ~ 70% in November (excluding rainy days). During the entire measurement period, ClNO_2 concentrations exhibited significant variability, with elevated levels (> 500 ppt) frequently observed in late autumn, particularly after November 10th. The elevation of ClNO_2 concentrations coincided with increased levels of N_2O_5 and NO_3^- during late autumn. The concentrations of ClNO_2 at our study site reached several ppb, compared with previous field measurements conducted at urban, suburban, rural, background, and mountain sites (Table S3), indicating its widespread presence in diverse atmospheric environments. The highest concentrations of ClNO_2 were detected during the night of November 27th, with a maximum hourly average of 3.4 ppb. Peak concentrations of N_2O_5 and NO_3^- were also observed on that night (Fig. 1). On the evening of November 27th, N_2O_5 concentrations rapidly decreased after 7 p.m., while ClNO_2 and NO_3^- concentrations significantly increased, reflecting fast N_2O_5 heterogeneous hydrolysis and effective formation of ClNO_2 . Notably, on the following day (November 28th) (Fig. 2a), ClNO_2 concentrations sustained above 100 ppt around noon, partially related with weakened UV values ($\sim 14 \text{ W}\cdot\text{m}^{-2}$) under heavy fog and cloud

cover, with the RH values of $\sim 70\%$ at that time. Similar research in California has shown ClNO₂ concentrations exceeding 100 ppt after sunrise 4 hours due to reduced photolysis (Mielke et al., 2013).

The average diurnal changes of ClNO₂ and related parameters during the entire measurement campaign are depicted in Fig. 2b. As expected, ClNO₂ exhibited a distinct diurnal variation, peaking and accumulating after sunset and decreasing in the early morning. However, ClNO₂ concentrations remained ~ 40 ppt around noon, different with some studies that ClNO₂ concentrations decreased to near the detection limit around midday (Wang et al., 2022; Niu et al., 2022). Similar observation in North China declared ClNO₂ concentrations above 60 ppt in the afternoon (Liu et al., 2017). Previous studies have indicated that abundant ClNO₂ may be transported from upper atmosphere or air mass, contributing to the elevated ClNO₂ concentrations in the early morning (Tham et al., 2016; Xia et al., 2021; Jeong et al., 2019). However, the explanations for the concentrations of ClNO₂ around noon remained elusive.

To evaluate the contribution of the heterogeneous N₂O₅ uptake to daytime ClNO₂ levels, we calculated ClNO₂ production using Eq. (S7), considering the loss of ClNO₂ through photolysis. This method has been employed in a previous study (Text S4-S5) (Tham et al., 2016). We used a $\gamma(\text{N}_2\text{O}_5)$ value of 0.06 and a $\phi(\text{ClNO}_2)$ value of 1.0 in our calculations, which represent upper-end estimates based on previous field studies (McDuffie et al., 2018a; McDuffie et al., 2018b; Tham et al., 2016). However, as shown in Fig. 3, the calculated $\phi(\text{ClNO}_2)$ with $\gamma(\text{N}_2\text{O}_5) = 0.06$ fails to reproduce the observed levels of daytime ClNO₂. A larger $\gamma(\text{N}_2\text{O}_5)$ of 0.11 would be necessary, but such high uptake coefficients and yields are not supported by the current literature. Therefore, we believe that the observed daytime ClNO₂ levels, particularly around noon, cannot be adequately explained by heterogeneous N₂O₅ uptake alone, suggesting the presence of additional sources contributing to the formation of daytime ClNO₂.

3.2 Key drivers of ClNO₂ formation

The XGBoost-SHAP model was employed to investigate the major drivers of ClNO₂ production during the whole observation period. The average absolute SHAP value of each feature was ranked to determine the key drivers of ClNO₂ formation, with larger SHAP values suggesting greater contributions (Fig. 4a). Additionally, features with positive SHAP values (depicted as red points) indicate that higher values of those features positively affect ClNO₂ concentrations, and vice versa (Fig. 4b). Overall, N₂O₅, NO₃⁻, T, RH, and UV were the most important features affecting ClNO₂ concentrations. Notably, these factors exhibited varied behaviors between daytime and nighttime periods.

In our study, N₂O₅ was identified as the most important influencing factor, consistent with its role in

ClNO₂ formation through heterogeneous uptake processes (Thornton et al., 2010; Finlayson-Pitts et al., 1989). After sunset, ClNO₂ concentrations markedly increased due to active nighttime N₂O₅ chemistry, while this heterogeneous uptake process was hindered after sunrise as N₂O₅ concentrations decreased significantly (Fig. 1) (Niu et al., 2022; Wang et al., 2020; Tan et al., 2022). Indeed, the concentrations of ClNO₂ were evidently increased when N₂O₅ concentrations exceeded ~13 ppt, predominantly during the nighttime (Fig. 5a). Conversely, in Northern Europe, the ClNO₂ concentrations were mainly controlled by O₃ and NO₂, rather than by the heterogeneous uptake of N₂O₅ (Sommariva et al., 2018). In Heshan of South China, chloride and PM_{2.5} were the major factors affecting ClNO₂ formation (Wang et al., 2022). Differently, the relative importance of NO₃⁻ derived from the XGBoost-SHAP result indicated that elevated ClNO₂ concentrations were associated with high concentrations of NO₃⁻ besides N₂O₅. According to Fig. 5b, high NO₃⁻ concentrations (> 3.7 μg·m⁻³) are accompanied by the elevation of ClNO₂, especially its concentrations reaching 6.2 μg·m⁻³. Previous studies suggested that increased concentrations of NO₃⁻ decreased γ(N₂O₅), which would limit the production of ClNO₂ (Wahner et al., 1998; Mentel et al., 1999; Bertram and Thornton, 2009). As depicted in Fig. S4, the dependence of γ(N₂O₅) on NO₃⁻ concentrations follows the nitrate suppression effect. Therefore, the importance of nighttime NO₃⁻ for ClNO₂ levels is that they are co-products from the processes of N₂O₅ heterogeneous uptake. As shown in Fig. 1, compared to low NO₃⁻ conditions, ClNO₂ production was enhanced in high NO₃⁻ conditions. Especially in late autumn, increased aerosol abundances and N₂O₅ levels increased N₂O₅ uptake further promoting ClNO₂ and NO₃⁻ production. Considering the limited contribution of N₂O₅ hydrolysis to daytime NO₃⁻ levels (Yan et al., 2023; Zang et al., 2022; Chen et al., 2020), the impact of high NO₃⁻ concentrations on daytime ClNO₂ concentrations warrants further analysis.

The simulated concentrations of ClNO₂, based on the XGBoost-SHAP model, were significantly elevated when NO₃⁻ concentrations were higher than 3.7 μg·m⁻³ (Fig. 5b). Consequently, the average daily concentrations of NO₃⁻ were classified as high (> 3.7 μg·m⁻³) and low (< 3.7 μg·m⁻³) to further elucidate the impacts of NO₃⁻ on the formation of ClNO₂. Fig. 6 presents the diurnal variations in the relative importance of factors based on the SHAP values under high and low NO₃⁻ concentrations. Unexpectedly, daytime NO₃⁻ was the dominant influencing factors for daytime ClNO₂ (Fig. 6a). High concentrations of daytime NO₃⁻ positively affected the daytime concentrations of ClNO₂, independent of N₂O₅ uptake processes. As depicted in Fig. 6a, daytime N₂O₅ did not promote the elevation of daytime ClNO₂. Negative SHAP values for N₂O₅ during the daytime indicate that the contribution of N₂O₅ chemistry to daytime ClNO₂ levels was limited. Therefore, it is very likely that high concentrations of daytime NO₃⁻ participated in daytime ClNO₂

production. A recent study suggested that nitrate photolysis produced ClNO₂ in addition to Cl₂ (Dalton et al., 2023), while it has been not verified by field observations. Fig. 7 shows that daytime ClNO₂ concentrations correlated well ($R=0.62$) with the product of a proxy of NO₃⁻ photolysis ($\text{NO}_3^- \times J\text{NO}_2 \times S_a$) on aerosol surfaces (S_a), implying that the photolysis of NO₃⁻ contributed to the daytime concentrations of ClNO₂ at our study site. Furthermore, high concentrations of NO₃⁻ and Cl⁻, along with large values of S_a (Fig. 7a, b, c) in the daytime accelerated NO₃⁻ photolysis, promoting the formation of ClNO₂. Overall, N₂O₅ uptake processes were the major pathways dominating nighttime ClNO₂ formation, while NO₃⁻ photolysis contributed to daytime ClNO₂ production during our observation period.

In term of meteorological factors, UV, T, and RH were the major influencing factors. The photolysis was the most important sink of ClNO₂ in the daytime, leading to a rapid reduction in ClNO₂ concentrations, particularly in the early morning (Fig. 5e and Fig. 6). However, it is crucial to understand the dual role of photolysis intensity in determining daytime ClNO₂ levels. Photolysis can contribute to the generation of ClNO₂ by promoting NO₃⁻ photolysis, while also causing the rapid decomposition of ClNO₂. As reported in California (Mielke et al., 2013), reduced photolysis rates even increased daytime ClNO₂ levels by decreasing ClNO₂ loss through photolysis. The impact of ambient temperature on ClNO₂ was probably reflected in its thermal equilibrium with N₂O₅. Elevated daytime ambient temperature suppressed the formation of N₂O₅, resulting in low N₂O₅ concentrations, which further limited the contribution of heterogeneous N₂O₅ uptake to daytime ClNO₂ generation (Fig. 5c and Fig. 6). During the whole observation period from October to November, the drop in ambient temperature facilitated ClNO₂ production by decreasing the thermal decomposition process. Increased RH values provided favorable conditions for the nighttime N₂O₅ hydrolysis reactions, thereby affecting ClNO₂ production (Fig. 5d and Fig. 6), while high RH (> 80%) also weakened the generation of ClNO₂. Notably, Cl⁻ was not the most important factors of ClNO₂ formation at our study site (Fig. 4), likely attributed to the abundant chlorine source in coastal regions (Peng et al., 2022).

3.3 Impact of ClNO₂ photolysis on RO_x budget

The photochemical effects of ClNO₂ were evaluated under the observation-average condition and the high ClNO₂ case based on the box model. The largest Cl production rates ($P(\text{Cl})$) contributed from ClNO₂ photolysis were 0.05 ppb·h⁻¹ for the observation-average condition, which was lower than 0.19 ppb·h⁻¹ for the high ClNO₂ case. The difference led to variable levels of atmospheric oxidation capacity induced by Cl radical. Cl radical released via the photolysis of ClNO₂ initiated the oxidation of VOCs. Among VOC groups (including alkanes, alkenes, alkynes, aromatics and OVOCs), Cl radical primarily oxidized alkanes

(~ 65.0%), followed by OVOCs (~ 12.7%) for both the observation-average condition and the high ClNO₂ case (Fig. 8a, b). The contributions of Cl radical and other atmospheric oxidants (including OH radical and O₃) to daytime VOC oxidation were also compared (Fig. 8c, d and Table 1). In our study, the oxidation of alkanes by Cl radical for the observation-average condition were about 11.7%, which increased by 44.8% for the high ClNO₂ case, were higher than those in London (Bannan et al., 2015), Weybourne (Bannan et al., 2017), Boston (Rutherford et al., 1995), and LA (Fraser et al., 1997), lower than that in Hong Kong (Xue et al., 2015). It should be noticed that the rates of Cl radical reacting with alkanes even exceeded those of OH radical in the early morning for the high ClNO₂ case. The largest rates of alkanes oxidized by Cl radical were approximately twice as high as those of OH radical at 10 a.m. (Fig. 8e, f), highlighting that the photochemical effects of Cl radical released via ClNO₂ photolysis were particularly important for VOC oxidation during the morning hours at our study site.

The oxidation of VOCs by Cl radical further affects the generation of RO_x (OH + HO₂ + RO₂) radicals. The RO_x radical production rates for the high ClNO₂ case were evidently lower than that under the observation-average condition, primarily due to reduced photolysis rates on that day. However, the total RO_x radical production rates averagely increased by 23.8% with ClNO₂ photolysis for the high ClNO₂ case, higher than a 4.9% increase for the observation-average condition (Fig. S5). For the observation-average condition, O₃ (32.7%), HONO (31.7%), and OVOCs (21.6%) photolysis were the most significant contributors to RO_x radical production in the early morning (7-10 a.m.), with VOC oxidation by Cl radical contributing only 3.7% (Fig. 9a). However, for the high ClNO₂ case, VOC oxidation induced by Cl radical in the early morning accounted for 19.1% of RO_x radical production, which was higher than O₃ (7.4%) and HCHO (4.1%) photolysis, close to OVOCs (19.0%) photolysis (Fig. 9b). The contributions of ClNO₂ photolysis to the RO_x radical production rates in our study were larger than previous results observed in autumn of Heshan (Wang et al., 2022) and North China (Xia et al., 2021), similar with that in summer of Wangdu (Tham et al., 2016). Thus, the concentrations of OH, HO₂, and RO₂ radicals in the box model with ClNO₂ inputs averagely increased by 17.9%, 34.6%, and 54.3% for the high ClNO₂ case, higher than the increases of 3.7%, 7.1%, and 10.3% contributed from the observation-average conditions, respectively (Fig. S6). The uplift in the concentrations of RO_x radicals also accelerated the generation of O₃. The increase in the net O₃ production rates (P(O₃)) for the observation-average condition averagely reached 0.13 ppb·h⁻¹ (15.8 %) in the daytime (Fig. 10a), while larger elevations in the net P(O₃) were observed for the high ClNO₂ case (Fig. 10b), with a maximum of 0.64 ppb·h⁻¹ (120 %) at 10 a.m. As a result, increased RO_x radical and O₃ greatly enhanced the atmospheric oxidation capacity (Fig. 10c, d), especially for the high

310 ClNO₂ case (up to 65%).

311 Table 2 summarizes the impacts of ClNO₂ photolysis on RO_x radical and O₃ production in our study
312 and previous observations around the world (Xia et al., 2021; Wang et al., 2022; Tham et al., 2016; Wang et
313 al., 2016; Xue et al., 2015; Bannan et al., 2017; Jeong et al., 2019), indicating that the photochemical
314 impacts of ClNO₂ were variable in different atmospheric environments. At our study site, the effects of
315 ClNO₂ photolysis on RO_x radical production were important, especially in the early morning. The enhanced
316 RO_x radical production induced by ClNO₂ photolysis accelerated the chemical generation of O₃. Primary
317 RO_x radical production rates (including O₃, HONO, HCHO, OVOCs, and ClNO₂) were considered as one of
318 the most important parameters to O₃ formation (Lu et al., 2023). Therefore, the considerable contribution of
319 ClNO₂ photolysis to primary RO_x radical production in the early morning may bring new challenges for O₃
320 alleviation.

322 Conclusions

323 In conclusion, we present two months of field measurements in the coastal area of Southern China
324 during the autumn, coupled with machine learning and model simulations, providing new insights into
325 ClNO₂ chemistry. Our observation shows the increase in the concentrations of ClNO₂ were accompanied by
326 elevated concentrations of N₂O₅ and NO₃⁻, low values of T and UV, and high values of RH. The nighttime
327 heterogeneous uptake of N₂O₅ was identified as the major source of ClNO₂, while NO₃⁻ photolysis
328 promoted the elevation of daytime ClNO₂ concentrations. Cl radical released by ClNO₂ photolysis after
329 sunrise had important photochemical effects in the early morning. The photolysis of high ClNO₂
330 concentrations resulted in net O₃ production rates and atmospheric oxidation capacity levels increasing by
331 120% and 65%, respectively. Our results enhanced the understanding of ClNO₂ chemistry in coastal regions,
332 calling for more observations and laboratory research to fully reveal its exact role in different atmospheric
333 environments.

335 **Data availability.** Data are available upon request to Jinsheng Chen (jschen@iue.ac.cn).

336
337 **Author contributions.** JC provided funding support for field measurements, designed this study, and
338 revised this manuscript. GC designed this study, analyzed the data, and wrote this manuscript. HW helped
339 perform the calibrations and revised this manuscript. XF revised this manuscript. XF, HW, YT, ZL, XJ, LX,
340 BH contributed to discussions of this manuscript.

Competing interests. The authors declare that they have no conflict of interest.

Acknowledgements. The authors acknowledge the National Natural Science Foundation of China, the Science and Technology Department of Fujian Province, Center for Excellence in Regional Atmospheric Environment Project, Xiamen Atmospheric Environment Observation and Research Station of Fujian Province, and Fujian Key Laboratory of Atmospheric Ozone Pollution Prevention (Institute of Urban Environment, Chinese Academy of Sciences).

Financial support. This work was funded by the National Natural Science Foundation of China (U22A20578, 42305102 & 42277091), the Science and Technology Department of Fujian Province (2022L3025), the National Key Research and Development Program (2022YFC3700304), STS Plan Supporting Project of the Chinese Academy of Sciences in Fujian Province (2023T3013), Fujian Provincial Environmental Protection Science & Technology Plan Projects (2023R004), and Xiamen Atmospheric Environment Observation and Research Station of Fujian Province. Y.J.T. acknowledges the funding support from the Guangdong Basic and Applied Basic Research Foundation (2022A1515010852) and the Fundamental Research Funds for the Central Universities, Sun Yat-sen University (23hytd002).

References

Atkinson, R., Baulch, D. L., Cox, R. A., Crowley, J. N., Hampson, R. F., Hynes, R. G., Jenkin, M. E., Rossi, M. J., Troe, J., and Subcommittee, I.: Evaluated kinetic and photochemical data for atmospheric chemistry: Volume II – gas phase reactions of organic species, *Atmos. Chem. Phys.*, 6, 3625-4055, <https://doi.org/10.5194/acp-6-3625-2006>, 2006.

Bannan, T. J., Bacak, A., Le Breton, M., Flynn, M., Ouyang, B., McLeod, M., Jones, R., Malkin, T. L., Whalley, L. K., Heard, D. E., Bandy, B., Khan, M. A. H., Shallcross, D. E., and Percival, C. J.: Ground and Airborne U.K. Measurements of Nitryl Chloride: An Investigation of the Role of Cl Atom Oxidation at Weybourne Atmospheric Observatory, *J. Geophys. Res. Atmos.*, 122, 11,154-111,165, <https://doi.org/10.1002/2017jd026624>, 2017.

Bannan, T. J., Booth, A. M., Bacak, A., Muller, J. B. A., Leather, K. E., Le Breton, M., Jones, B., Young, D., Coe, H., Allan, J., Visser, S., Slowik, J. G., Furger, M., Prévôt, A. S. H., Lee, J., Dunmore, R. E., Hopkins, J.

371 R., Hamilton, J. F., Lewis, A. C., Whalley, L. K., Sharp, T., Stone, D., Heard, D. E., Fleming, Z. L., Leigh,
 372 R., Shallcross, D. E., and Percival, C. J.: The first UK measurements of nitryl chloride using a chemical
 373 ionization mass spectrometer in central London in the summer of 2012, and an investigation of the role of Cl
 374 atom oxidation, *J. Geophys. Res. Atmos.*, 120, 5638-5657, <https://doi.org/10.1002/2014jd022629>, 2015.

375 Bertram, T. and Thornton, J.: Toward a general parameterization of N₂O₅ reactivity on aqueous particles: the
 376 competing effects of particle liquid water, nitrate and chloride, *Atmos. Chem. Phys.*, 9, 8351-8363,
 377 <https://doi.org/10.5194/acp-9-8351-2009>, 2009.

378 Chen, G., Ji, X., Chen, J., Xu, L., Hu, B., Lin, Z., Fan, X., Li, M., Hong, Y., and Chen, J.: Photochemical
 379 pollution during summertime in a coastal city of Southeast China: Ozone formation and influencing factors,
 380 *Atmos. Res.*, 301, 107270, <https://doi.org/10.1016/j.atmosres.2024.107270>, 2024.

381 Chen, X., Wang, H., Lu, K., Li, C., Zhai, T., Tan, Z., Ma, X., Yang, X., Liu, Y., Chen, S., Dong, H., Li, X.,
 382 Wu, Z., Hu, M., Zeng, L., and Zhang, Y.: Field Determination of Nitrate Formation Pathway in Winter
 383 Beijing, *Environ. Sci. Technol.*, 54, 9243-9253, <https://doi.org/10.1021/acs.est.0c00972>, 2020.

384 Dalton, E. Z., Hoffmann, E. H., Schaefer, T., Tilgner, A., Herrmann, H., and Raff, J. D.: Daytime
 385 Atmospheric Halogen Cycling through Aqueous-Phase Oxygen Atom Chemistry, *J. Am. Chem. Soc.*, 145,
 386 15652-15657, <https://doi.org/10.1021/jacs.3c03112>, 2023.

387 Finlayson-Pitts, B. J., Ezell, M. J., and Pitts, J. N.: Formation of chemically active chlorine compounds by
 388 reactions of atmospheric NaCl particles with gaseous N₂O₅ and ClONO₂, *Nature.*, 337, 241-244,
 389 <https://doi.org/10.1038/337241a0>, 1989.

390 Fraser, M. P., Cass, G. R., Simoneit, B. R., and Rasmussen, R.: Air quality model evaluation data for
 391 organics. 4. C₂–C₃₆ non-aromatic hydrocarbons, *Environ. Sci. Technol.*, 31, 2356-2367,
 392 <https://doi.org/10.1021/es960980g>, 1997.

393 Hu, B., Duan, J., Hong, Y., Xu, L., Li, M., Bian, Y., Qin, M., Fang, W., Xie, P., and Chen, J.: Exploration of
 394 the atmospheric chemistry of nitrous acid in a coastal city of southeastern China: results from measurements
 395 across four seasons, *Atmos. Chem. Phys.*, 22, 371-393, <https://doi.org/10.5194/acp-22-371-2022>, 2022.

396 Jeong, D., Seco, R., Gu, D., Lee, Y., Nault, B. A., Knote, C. J., McGee, T., Sullivan, J. T., Jimenez, J. L.,
 397 Campuzano-Jost, P., Blake, D. R., Sanchez, D., Guenther, A. B., Tanner, D., Huey, L. G., Long, R.,

Anderson, B. E., Hall, S. R., Ullmann, K., Shin, H., Herndon, S. C., Lee, Y., Kim, D., Ahn, J., and Kim, S.:
 Integration of airborne and ground observations of nitryl chloride in the Seoul metropolitan area and the
 implications on regional oxidation capacity during KORUS-AQ 2016, *Atmos. Chem. Phys.*, 19, 12779-
 12795, <https://doi.org/10.5194/acp-19-12779-2019>, 2019.

Li, F., Huang, D. D., Nie, W., Tham, Y. J., Lou, S., Li, Y., Tian, L., Liu, Y., Zhou, M., and Wang, H.:
 Observation of nitrogen oxide-influenced chlorine chemistry and source analysis of Cl₂ in the Yangtze River
 Delta, China, *Atmos. Environ.*, 306, 119829, <https://doi.org/10.1016/j.atmosenv.2023.119829>, 2023.

Li, Q., Badia, A., Wang, T., Sarwar, G., Fu, X., Zhang, L., Zhang, Q., Fung, J., Cuevas, C. A., Wang, S.,
 Zhou, B., and Saiz-Lopez, A.: Potential Effect of Halogens on Atmospheric Oxidation and Air Quality in
 China, *J. Geophys. Res. Atmos.*, 125, e2019JD032058, <https://doi.org/10.1029/2019JD032058>, 2020.

Liu, T., Chen, G., Chen, J., Xu, L., Li, M., Hong, Y., Chen, Y., Ji, X., Yang, C., Chen, Y., Huang, W., Huang,
 Q., and Wang, H.: Seasonal characteristics of atmospheric peroxyacetyl nitrate (PAN) in a coastal city of
 Southeast China: Explanatory factors and photochemical effects, *Atmos. Chem. Phys.*, 22, 4339-4353,
<https://doi.org/10.5194/acp-22-4339-2022>, 2022a.

Liu, T., Hong, Y., Li, M., Xu, L., Chen, J., Bian, Y., Yang, C., Dan, Y., Zhang, Y., Xue, L., Zhao, M., Huang,
 Z., and Wang, H.: Atmospheric oxidation capacity and ozone pollution mechanism in a coastal city of
 southeastern China: analysis of a typical photochemical episode by an observation-based model, *Atmos.*
Chem. Phys., 22, 2173-2190, <https://doi.org/10.5194/acp-22-2173-2022>, 2022b.

Liu, X., Qu, H., Huey, L. G., Wang, Y., Sjostedt, S., Zeng, L., Lu, K., Wu, Y., Hu, M., Shao, M., Zhu, T., and
 Zhang, Y.: High Levels of Daytime Molecular Chlorine and Nitryl Chloride at a Rural Site on the North
 China Plain, *Environ. Sci. Technol.*, 51, 9588-9595, <https://doi.org/10.1021/acs.est.7b03039>, 2017.

Lu, K., Zhou, H., Lee, J., Nelson, B., and Zhang, Y.: Ozone mitigations beyond the control of nitrogen
 oxides and volatile organic compounds, *Sci Bull*, 68, 1989-1992, <https://doi.org/10.1016/j.scib.2023.07.051>,
 2023.

Ma, W., Chen, X., Xia, M., Liu, Y., Wang, Y., Zhang, Y., Zheng, F., Zhan, J., Hua, C., and Wang, Z.:
 Reactive Chlorine Species Advancing the Atmospheric Oxidation Capacities of Inland Urban Environments,
Environ. Sci. Technol., 57, 14638-14647, <https://doi.org/10.1021/acs.est.3c05169>, 2023.

McDuffie, E. E., Fibiger, D. L., Dubé, W. P., Lopez Hilfiker, F., Lee, B. H., Jaeglé, L., Guo, H., Weber, R. J.,
 Reeves, J. M., Weinheimer, A. J., Schroder, J. C., Campuzano-Jost, P., Jimenez, J. L., Dibb, J. E., Veres, P.,
 Ebben, C., Sparks, T. L., Wooldridge, P. J., Cohen, R. C., Campos, T., Hall, S. R., Ullmann, K., Roberts, J.
 M., Thornton, J. A., and Brown, S. S.: ClNO₂ Yields From Aircraft Measurements During the 2015
 WINTER Campaign and Critical Evaluation of the Current Parameterization, *J. Geophys. Res. Atmos.*, 123,
 12,994-913,015, <https://doi.org/10.1029/2018JD029358>, 2018a.

McDuffie, E. E., Fibiger, D. L., Dubé, W. P., Lopez-Hilfiker, F., Lee, B. H., Thornton, J. A., Shah, V., Jaeglé,
 L., Guo, H., Weber, R. J., Michael Reeves, J., Weinheimer, A. J., Schroder, J. C., Campuzano-Jost, P.,
 Jimenez, J. L., Dibb, J. E., Veres, P., Ebben, C., Sparks, T. L., Wooldridge, P. J., Cohen, R. C., Hornbrook, R.
 S., Apel, E. C., Campos, T., Hall, S. R., Ullmann, K., and Brown, S. S.: Heterogeneous N₂O₅ Uptake During
 Winter: Aircraft Measurements During the 2015 WINTER Campaign and Critical Evaluation of Current
 Parameterizations, *J. Geophys. Res. Atmos.*, 123, 4345-4372, <https://doi.org/10.1002/2018JD028336>, 2018b.

Mentel, T. F., Sohn, M., and Wahner, A. J. P. C. C. P.: Nitrate effect in the heterogeneous hydrolysis of
 dinitrogen pentoxide on aqueous aerosols, *Phys. Chem. Chem. Phys.*, 1, 5451-5457,
<https://doi.org/10.1039/A905338g>, 1999.

Mielke, L. H., Furgeson, A., and Osthoff, H. D.: Observation of ClNO₂ in a Mid-Continental Urban
 Environment, *Environ. Sci. Technol.*, 45, 8889-8896, <https://doi.org/10.1021/es201955u>, 2011.

Mielke, L. H., Stutz, J., Tsai, C., Hurlock, S. C., Roberts, J. M., Veres, P. R., Froyd, K. D., Hayes, P. L.,
 Cubison, M. J., Jimenez, J. L., Washenfelder, R. A., Young, C. J., Gilman, J. B., Gouw, J. A., Flynn, J. H.,
 Grossberg, N., Lefer, B. L., Liu, J., Weber, R. J., and Osthoff, H. D.: Heterogeneous formation of nitryl
 chloride and its role as a nocturnal NO_x reservoir species during CalNex-LA 2010, *J. Geophys. Res. Atmos.*,
 118, 10,638-610,652, <https://doi.org/10.1002/jgrd.50783>, 2013.

Niu, Y.-B., Zhu, B., He, L.-Y., Wang, Z., Lin, X.-Y., Tang, M.-X., and Huang, X.-F.: Fast Nocturnal
 Heterogeneous Chemistry in a Coastal Background Atmosphere and Its Implications for Daytime
 Photochemistry, *J. Geophys. Res. Atmos.*, 127, e2022JD036716, <https://doi.org/10.1029/2022JD036716>,
 2022.

Osthoff, H. D., Roberts, J. M., Ravishankara, A. R., Williams, E. J., Lerner, B. M., Sommariva, R., Bates, T.

452 S., Coffman, D., Quinn, P. K., Dibb, J. E., Stark, H., Burkholder, J. B., Talukdar, R. K., Meagher, J.,
 453 Fehsenfeld, F. C., and Brown, S. S.: High levels of nitryl chloride in the polluted subtropical marine
 454 boundary layer, *Nat. Geosci.*, 1, 324-328, <https://doi.org/10.1038/ngeo177>, 2008.

455 Peng, X., Wang, T., Wang, W., Ravishankara, A., George, C., Xia, M., Cai, M., Li, Q., Salvador, C. M., and
 456 Lau, C.: Photodissociation of particulate nitrate as a source of daytime tropospheric Cl₂, *Nat. Commun.*, 13,
 457 1-10, <https://doi.org/10.1038/s41467-022-28383-9>, 2022.

458 Peng, X., Wang, W., Xia, M., Chen, H., Ravishankara, A. R., Li, Q., Saiz-Lopez, A., Liu, P., Zhang, F.,
 459 Zhang, C., Xue, L., Wang, X., George, C., Wang, J., Mu, Y., Chen, J., and Wang, T.: An unexpected large
 460 continental source of reactive bromine and chlorine with significant impact on wintertime air quality, *Natl.*
 461 *Sci. Rev.*, 8, nwaa304, <https://doi.org/10.1093/nsr/nwaa304>, 2021.

462 Phillips, G. J., Tang, M. J., Thieser, J., Brickwedde, B., Schuster, G., Bohn, B., Lelieveld, J., and Crowley, J.
 463 N.: Significant concentrations of nitryl chloride observed in rural continental Europe associated with the
 464 influence of sea salt chloride and anthropogenic emissions, *Geophys. Res. Lett.*, 39, L10811,
 465 <https://doi.org/10.1029/2012gl051912>, 2012.

466 Riedel, T. P., Bertram, T. H., Crisp, T. A., Williams, E. J., Lerner, B. M., Vlasenko, A., Li, S. M., Gilman, J.,
 467 de Gouw, J., Bon, D. M., Wagner, N. L., Brown, S. S., and Thornton, J. A.: Nitryl chloride and molecular
 468 chlorine in the coastal marine boundary layer, *Environ. Sci. Technol.*, 46, 10463-10470,
 469 <https://doi.org/10.1021/es204632r>, 2012.

470 Rutherford, J. A., Koehl, W. J., Benson, J. D., Burns, V. R., Hochhauser, A. M., Knepper, J. C., Leppard, W.
 471 R., Painter, L. J., Rapp, L. A., and Rippon, B.: Effects of Gasoline Properties on Emissions of Current and
 472 Future Vehicles-T50, T90, and Sulfur Effects-Auto/Oil Air Quality Improvement Research Program, SAE
 473 Technical Paper0148-7191, <https://doi.org/10.4271/952510>, 1995.

474 Sommariva, R., Hollis, L. D. J., Sherwen, T., Baker, A. R., Ball, S. M., Bandy, B. J., Bell, T. G., Chowdhury,
 475 M. N., Cordell, R. L., Evans, M. J., Lee, J. D., Reed, C., Reeves, C. E., Roberts, J. M., Yang, M., and Monks,
 476 P. S.: Seasonal and geographical variability of nitryl chloride and its precursors in Northern Europe, *Atmos.*
 477 *Sci. Lett.*, 19, <https://doi.org/10.1002/asl.844>, 2018.

478 Tan, Z., Fuchs, H., Hofzumahaus, A., Bloss, W. J., Bohn, B., Cho, C., Hohaus, T., Holland, F., Lakshmisha,

479 C., Liu, L., Monks, P. S., Novelli, A., Niether, D., Rohrer, F., Tillmann, R., Valkenburg, T. S. E., Vardhan, V.,
 480 Kiendler-Scharr, A., Wahner, A., and Sommariva, R.: Seasonal variation in nitryl chloride and its relation to
 481 gas-phase precursors during the JULIAC campaign in Germany, *Atmos. Chem. Phys.*, 22, 13137-13152,
 482 <https://doi.org/10.5194/acp-22-13137-2022>, 2022.

483 Thaler, R. D., Mielke, L. H., and Osthoff, H. D.: Quantification of nitryl chloride at part per trillion mixing
 484 ratios by thermal dissociation cavity ring-down spectroscopy, *Anal. Chem.*, 83, 2761-2766,
 485 <https://doi.org/10.1021/ac200055z>, 2011.

486 Tham, Y. J., Wang, Z., Li, Q., Wang, W., Wang, X., Lu, K., Ma, N., Yan, C., Kecorius, S., Wiedensohler, A.,
 487 Zhang, Y., and Wang, T.: Heterogeneous N₂O₅ uptake coefficient and production yield of ClNO₂ in polluted
 488 northern China: roles of aerosol water content and chemical composition, *Atmos. Chem. Phys.*, 18, 13155-
 489 13171, <https://doi.org/10.5194/acp-18-13155-2018>, 2018.

490 Tham, Y. J., Wang, Z., Li, Q., Yun, H., Wang, W., Wang, X., Xue, L., Lu, K., Ma, N., Bohn, B., Li, X.,
 491 Kecorius, S., Größ, J., Shao, M., Wiedensohler, A., Zhang, Y., and Wang, T.: Significant concentrations of
 492 nitryl chloride sustained in the morning: investigations of the causes and impacts on ozone production in a
 493 polluted region of northern China, *Atmos. Chem. Phys.*, 16, 14959-14977, [https://doi.org/10.5194/acp-16-](https://doi.org/10.5194/acp-16-14959-2016)
 494 [14959-2016](https://doi.org/10.5194/acp-16-14959-2016), 2016.

495 Thornton, J. A., Braban, C. F., and Abbatt, J. P.: N₂O₅ hydrolysis on sub-micron organic aerosols: the effect
 496 of relative humidity, particle phase, and particle size, *Phys. Chem. Chem. Phys.*, 5, 4593-4603,
 497 <https://doi.org/10.1039/B307498F>, 2003.

498 Thornton, J. A., Kercher, J. P., Riedel, T. P., Wagner, N. L., Cozic, J., Holloway, J. S., Dubé, W. P., Wolfe, G.
 499 M., Quinn, P. K., Middlebrook, A. M., Alexander, B., and Brown, S. S.: A large atomic chlorine source
 500 inferred from mid-continental reactive nitrogen chemistry, *Nature.*, 464, 271-274,
 501 <https://doi.org/10.1038/nature08905>, 2010.

502 Wahner, A., Mentel, T. F., Sohn, M., and Stier, J.: Heterogeneous reaction of N₂O₅ on sodium nitrate aerosol,
 503 *J. Geophys. Res. Atmos.*, 103, 31103-31112, <https://doi.org/10.1029/1998JD100022>, 1998.

504 Wang, H., Yuan, B., Zheng, E., Zhang, X., Wang, J., Lu, K., Ye, C., Yang, L., Huang, S., and Hu, W.:
 505 Formation and impacts of nitryl chloride in Pearl River Delta, *Atmos. Chem. Phys.*, 22, 14837-14858,

506 <https://doi.org/10.5194/acp-22-14837-2022>, 2022.

507 Wang, H., Wang, H., Lu, X., Lu, K., Zhang, L., Tham, Y. J., Shi, Z., Aikin, K., Fan, S., Brown, S. S., and
508 Zhang, Y.: Increased night-time oxidation over China despite widespread decrease across the globe, *Nat.*
509 *Geosci.*, 16, 217-223, <https://doi.org/10.1038/s41561-022-01122-x>, 2023.

510 Wang, H., Chen, X., Lu, K., Tan, Z., Ma, X., Wu, Z., Li, X., Liu, Y., Shang, D., Wu, Y., Zeng, L., Hu, M.,
511 Schmitt, S., Kiendler-Scharr, A., Wahner, A., and Zhang, Y.: Wintertime N₂O₅ uptake coefficients over the
512 North China Plain, *Sci. Bull.*, 65, 765-774, <https://doi.org/10.1016/j.scib.2020.02.006>, 2020.

513 Wang, T., Tham, Y. J., Xue, L., Li, Q., Zha, Q., Wang, Z., Poon, S. C. N., Dubé, W. P., Blake, D. R., Louie, P.
514 K. K., Luk, C. W. Y., Tsui, W., and Brown, S. S.: Observations of nitryl chloride and modeling its source and
515 effect on ozone in the planetary boundary layer of southern China, *J. Geophys. Res. Atmos.*, 121, 2476-2489,
516 <https://doi.org/10.1002/2015JD024556>, 2016.

517 Wang, Z., Wang, W., Tham, Y. J., Li, Q., Wang, H., Wen, L., Wang, X., and Wang, T.: Fast heterogeneous
518 N₂O₅ uptake and ClNO₂ production in power plant and industrial plumes observed in the nocturnal residual
519 layer over the North China Plain, *Atmos. Chem. Phys.*, 17, 12361-12378, [https://doi.org/10.5194/acp-17-](https://doi.org/10.5194/acp-17-12361-2017)
520 [12361-2017](https://doi.org/10.5194/acp-17-12361-2017), 2017.

521 Xia, M., Peng, X., Wang, W., Yu, C., Wang, Z., Tham, Y. J., Chen, J., Chen, H., Mu, Y., and Zhang, C.:
522 Winter ClNO₂ formation in the region of fresh anthropogenic emissions: seasonal variability and insights
523 into daytime peaks in northern China, *Atmos. Chem. Phys.*, 21, 15985-16000, [https://doi.org/10.5194/acp-](https://doi.org/10.5194/acp-21-15985-2021)
524 [21-15985-2021](https://doi.org/10.5194/acp-21-15985-2021), 2021.

525 Xia, M., Peng, X., Wang, W., Yu, C., Sun, P., Li, Y., Liu, Y. A. H. C. t. A.-P. O. A. C., Xu, Z., Wang, Z., Xu,
526 Z., Nie, W., Ding, A., and Wang, T.: Significant production of ClNO₂ and possible source of Cl₂ from N₂O₅
527 uptake at a suburban site in eastern China, *Atmos. Chem. Phys.*, 20, 6147-6158, [https://doi.org/10.5194/acp-](https://doi.org/10.5194/acp-20-6147-2020)
528 [20-6147-2020](https://doi.org/10.5194/acp-20-6147-2020), 2020.

529 Xue, L. K., Saunders, S. M., Wang, T., Gao, R., Wang, X. F., Zhang, Q. Z., and Wang, W. X.: Development
530 of a chlorine chemistry module for the Master Chemical Mechanism, *Geosci. Model Dev.*, 8, 3151-3162,
531 <https://doi.org/10.5194/gmd-8-3151-2015>, 2015.

532 Yan, C., Tham, Y. J., Nie, W., Xia, M., Wang, H., Guo, Y., Ma, W., Zhan, J., Hua, C., and Li, Y.: Increasing

533 contribution of nighttime nitrogen chemistry to wintertime haze formation in Beijing observed during
 534 COVID-19 lockdowns, *Nat. Geosci.*, 16, 975-981, <https://doi.org/10.1038/s41561-023-01285-1>, 2023.

535 Yi, X., Sarwar, G., Bian, J., Huang, L., Li, Q., Jiang, S., Liu, H., Wang, Y., Chen, H., and Wang, T.:
 536 Significant Impact of Reactive Chlorine on Complex Air Pollution Over the Yangtze River Delta Region,
 537 China, *J. Geophys. Res. Atmos.*, 128, e2023JD038898, <https://doi.org/10.1029/2023JD038898>, 2023.

538 Yun, H., Wang, T., Wang, W., Tham, Y. J., Li, Q., Wang, Z., and Poon, S. C. N.: Nighttime NO_x loss and
 539 ClNO₂ formation in the residual layer of a polluted region: Insights from field measurements and an iterative
 540 box model, *Sci. Total Environ.*, 622-623, 727-734, <https://doi.org/10.1016/j.scitotenv.2017.11.352>, 2018a.

541 Yun, H., Wang, W., Wang, T., Xia, M., Yu, C., Wang, Z., Poon, S. C. N., Yue, D., and Zhou, Y.: Nitrate
 542 formation from heterogeneous uptake of dinitrogen pentoxide during a severe winter haze in southern China,
 543 *Atmos. Chem. Phys.*, 18, 17515-17527, <https://doi.org/10.5194/acp-18-17515-2018>, 2018b.

544 Zang, H., Zhao, Y., Huo, J., Zhao, Q., Fu, Q., Duan, Y., Shao, J., Huang, C., An, J., Xue, L., Li, Z., Li, C.,
 545 and Xiao, H.: High atmospheric oxidation capacity drives wintertime nitrate pollution in the eastern Yangtze
 546 River Delta of China, *Atmos. Chem. Phys.*, 22, 4355-4374, <https://doi.org/10.5194/acp-22-4355-2022>, 2022.

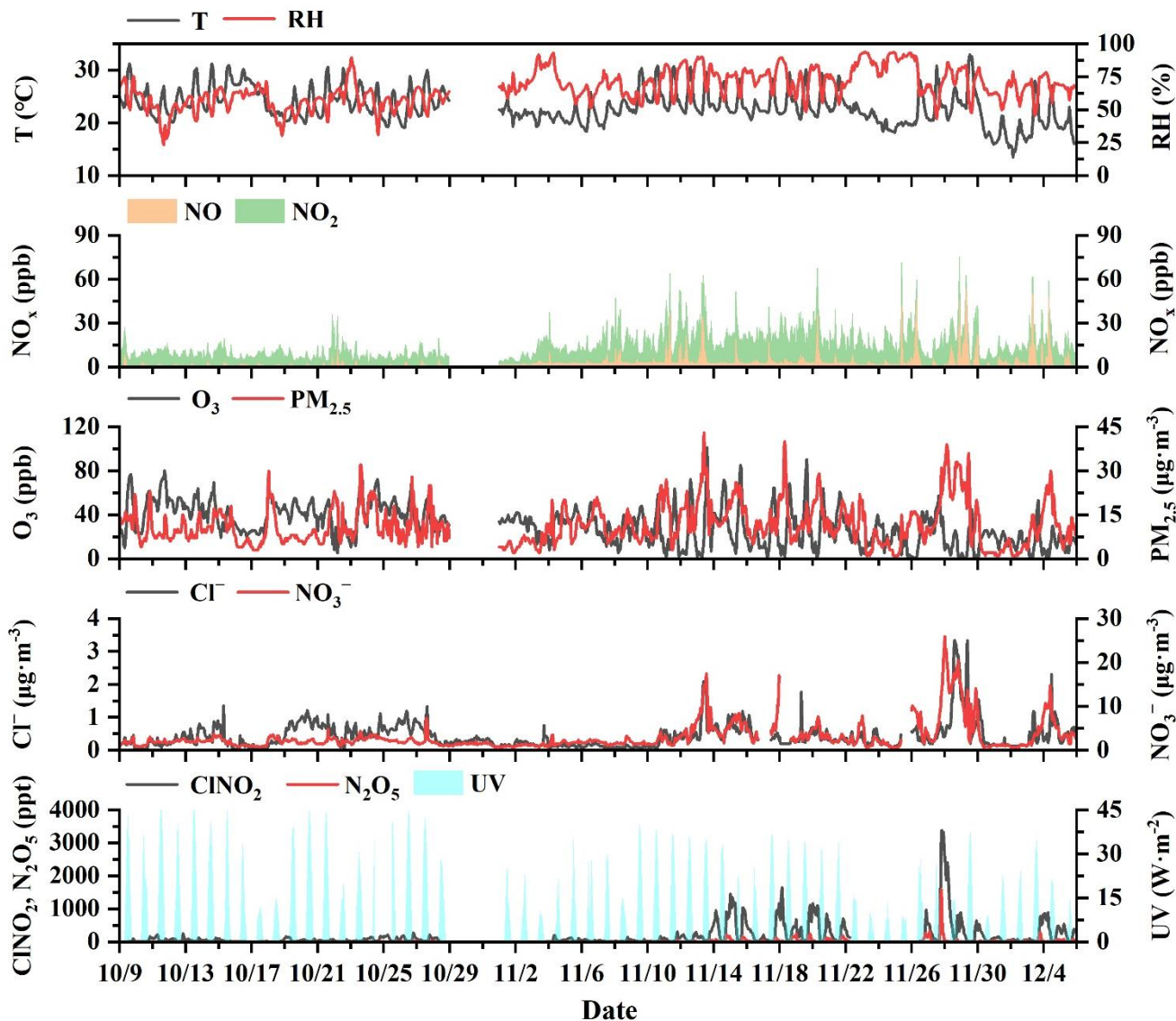


Figure 1. The time series of ClNO_2 , related precursors, and meteorological parameters during the autumn observation period.

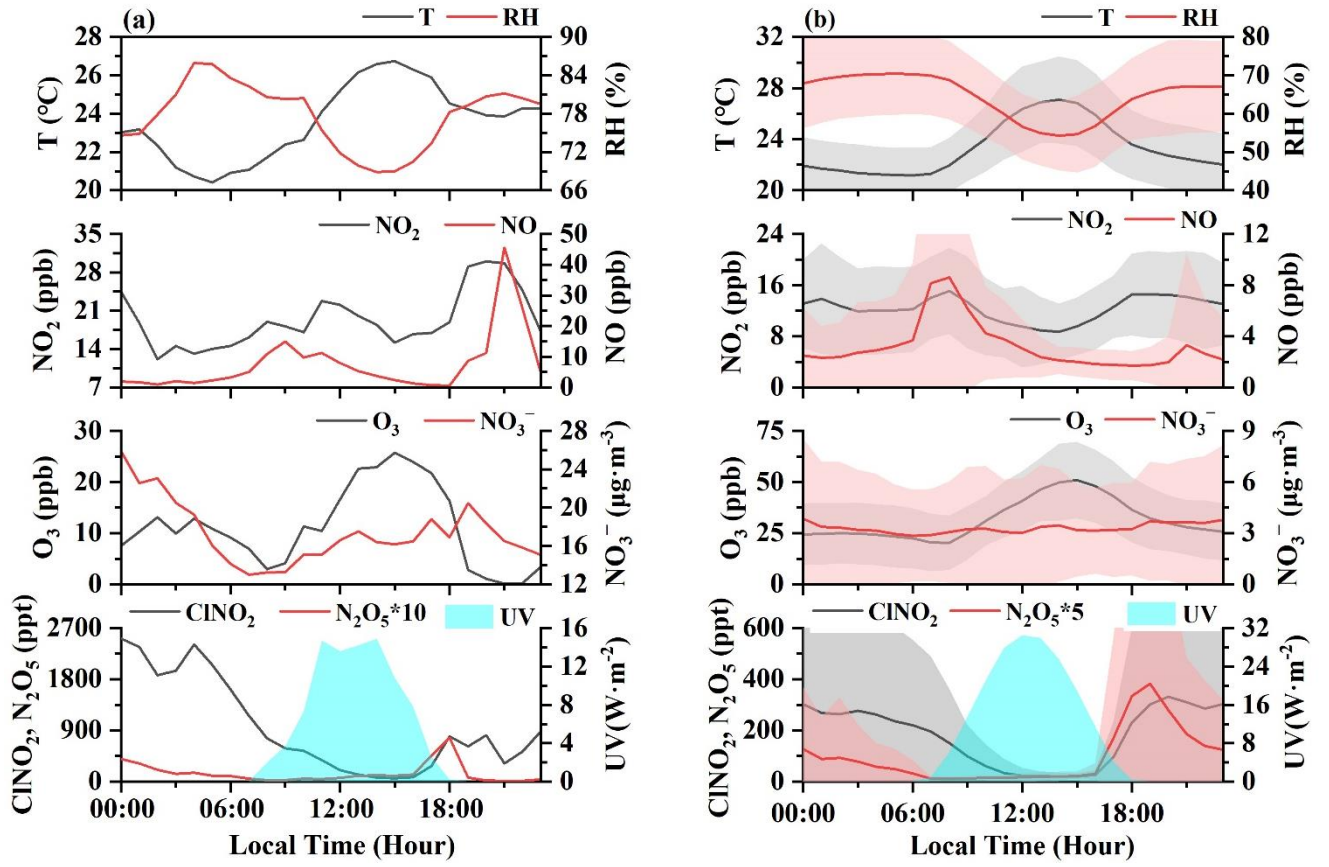


Figure 2. Diurnal variations of ClNO₂ and other related parameters for the highest concentrations of ClNO₂ (case) on November 28th (a) and the observation-average condition (from 9 October to 5 December) (b).

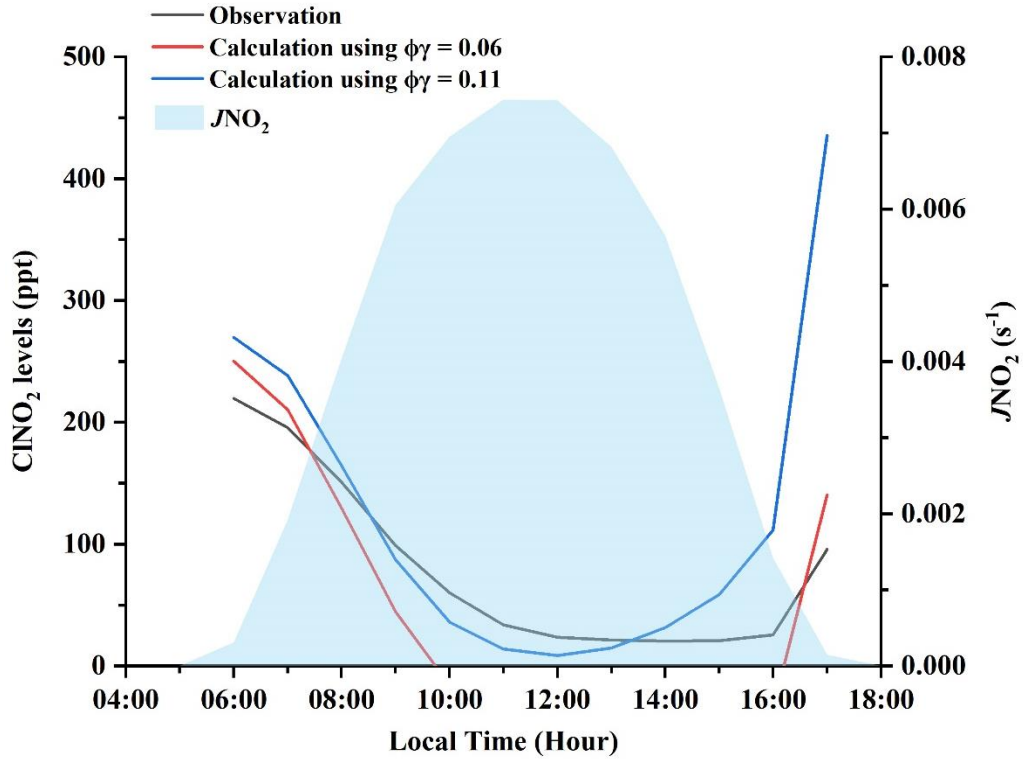


Figure 3. Comparisons of daytime ClNO_2 levels between observation, and calculation using Eq. (4) with a $\phi(\text{ClNO}_2)$ of 1.0 and a $\gamma(\text{N}_2\text{O}_5)$ of 0.06 ($\phi\gamma = 0.06$), or a $\phi(\text{ClNO}_2)$ of 1.0 and a $\gamma(\text{N}_2\text{O}_5)$ of 0.11 ($\phi\gamma = 0.11$).

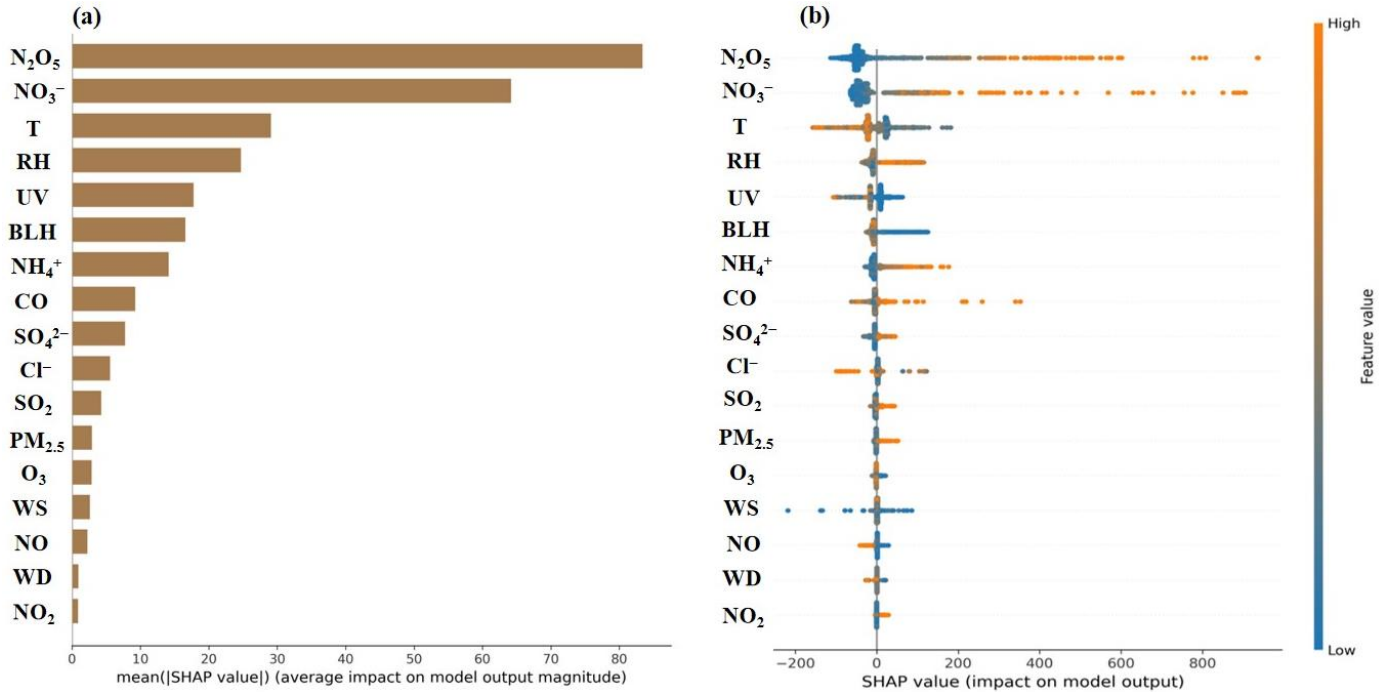


Figure 4. Relative importance of each feature to ClNO_2 using XGBoost-SHAP during the autumn observation period. The mean absolute SHAP value (a), summary plot of SHAP values of each feature (b).

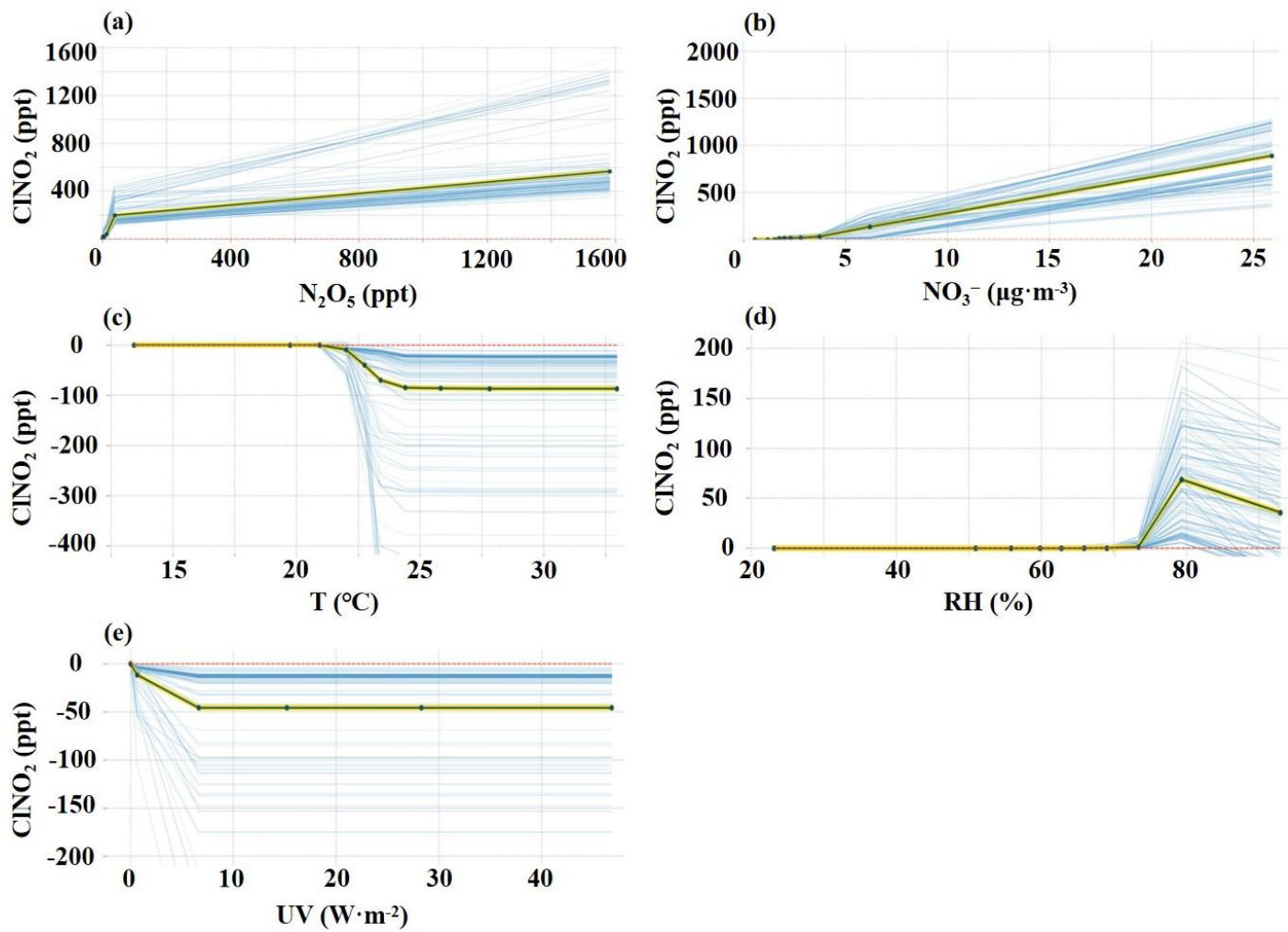


Figure 5. Isolation plots of PDP for N_2O_5 (a), NO_3^- (b), T (c), RH (d), and UV (e). The average variations of simulated ClNO_2 with factors' changes spline are indicated by the yellow and black curve, and blue curves presents all situations during the whole observation period.

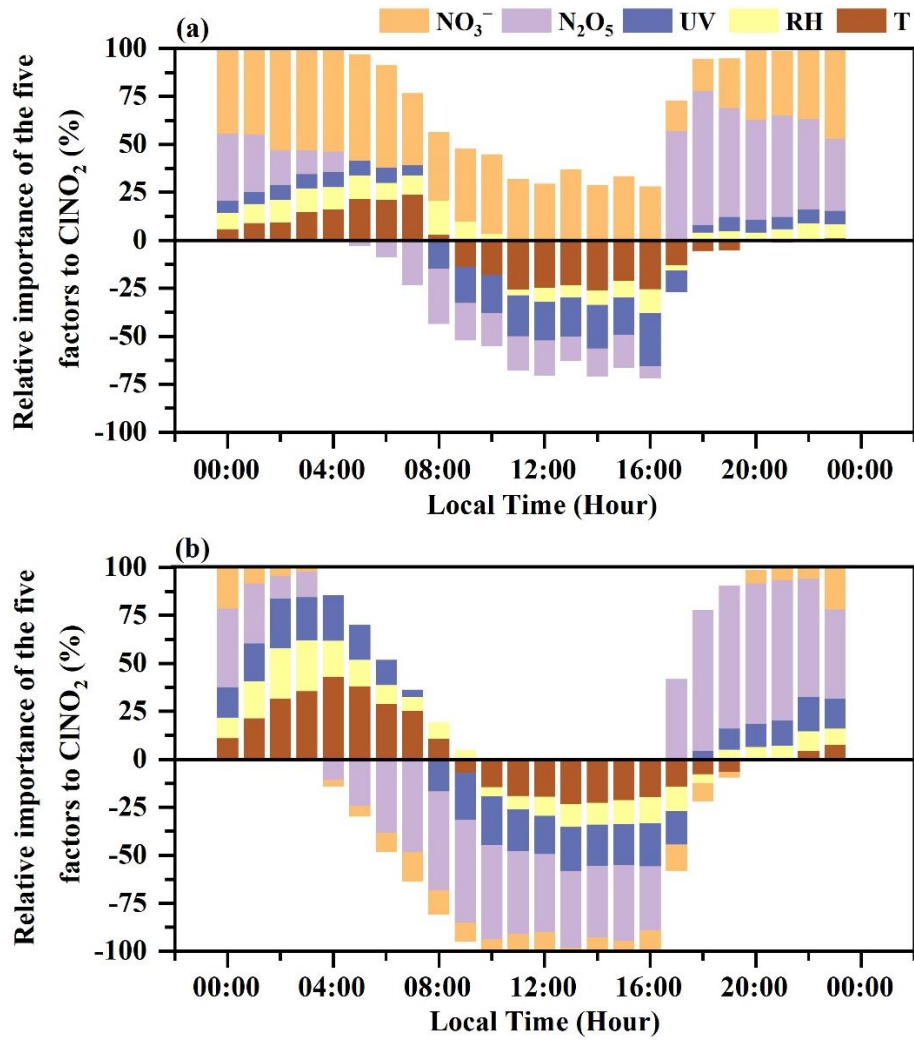


Figure 6. The diurnal variations of the relative importance of factors to ClNO_2 based on the SHAP values under the high ($> 3.7 \mu\text{g}\cdot\text{m}^{-3}$) (a) and low ($< 3.7 \mu\text{g}\cdot\text{m}^{-3}$) (b) ClNO_2 concentrations.

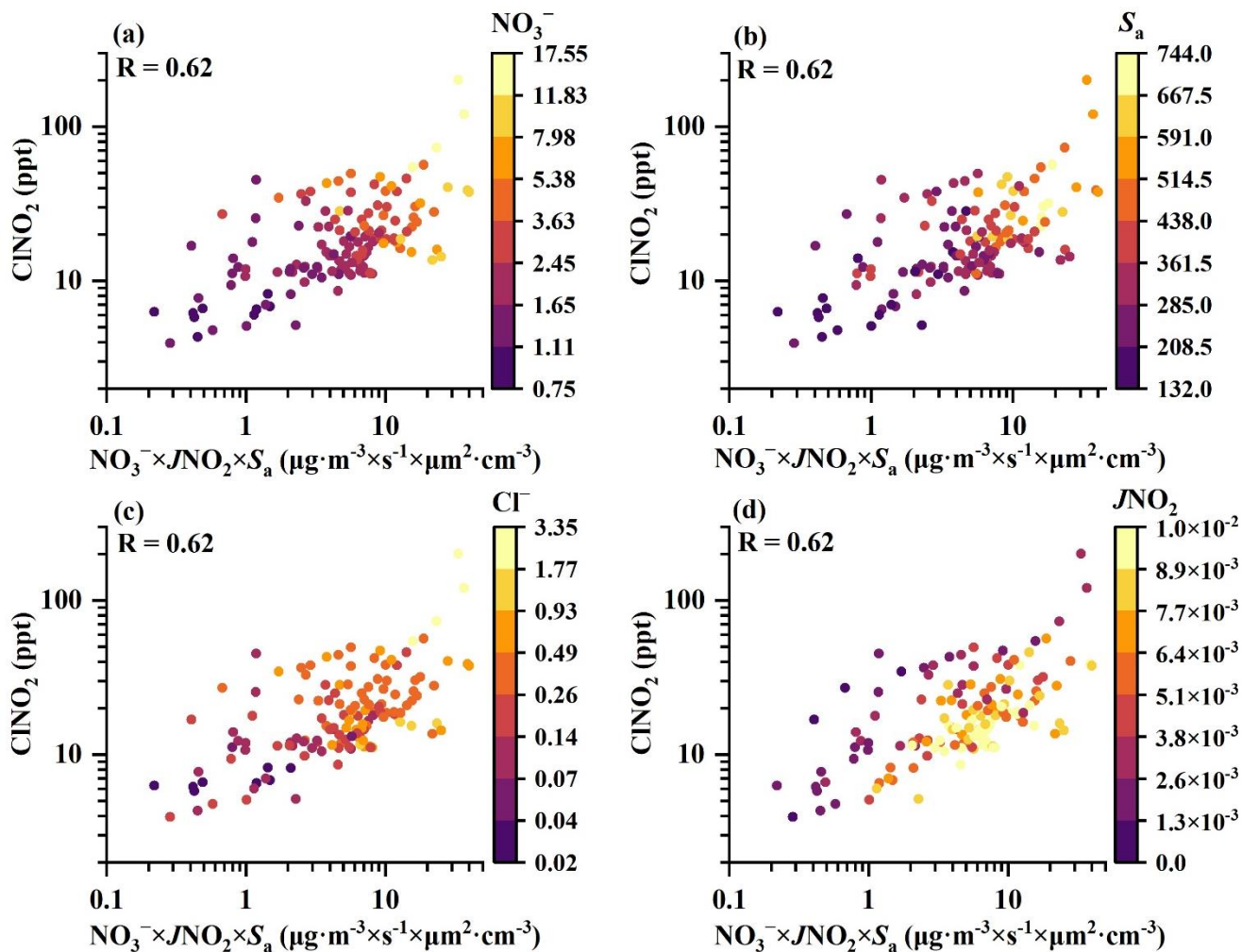


Figure 7. The relationship of daytime ClNO_2 concentrations (12:00-15:00 Local Time) and a proxy of nitrate (NO_3^-) photolysis ($\text{NO}_3^- \times J\text{NO}_2 \times S_a$). The color of the dots respects the NO_3^- (a), S_a (b), Cl^- (c), $J\text{NO}_2$ (d), respectively.

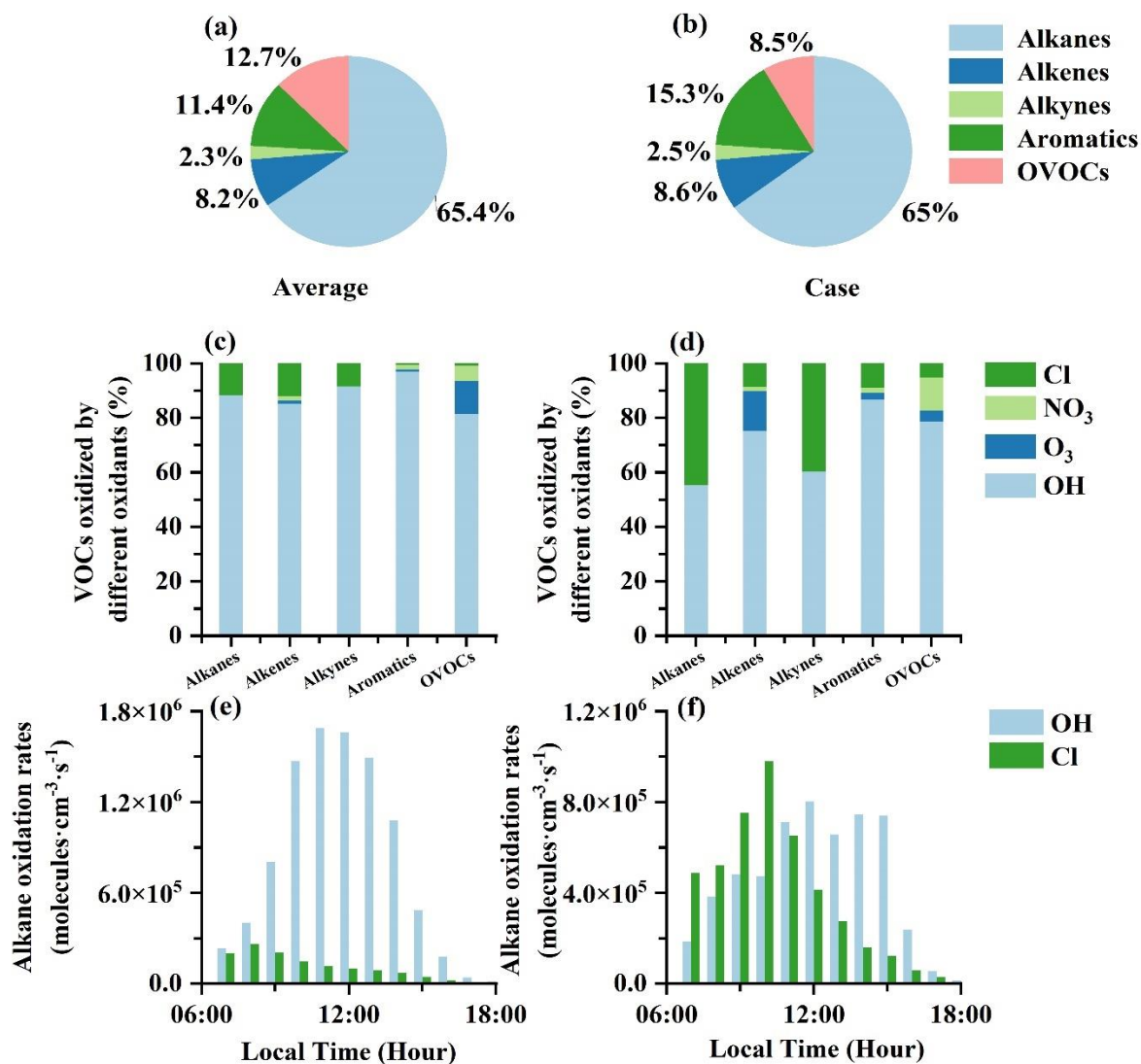


Figure 8. The impacts of Cl radicals released by ClNO₂ photolysis and other atmospheric oxidants (including OH, NO₃, and O₃) on VOC oxidation under the observation-average condition and high ClNO₂ case, respectively. The contributions of different VOC groups oxidized by Cl radical during the observation-average (a). The contributions of different VOC groups oxidized by Cl radical during the case (b). The contributions of different atmospheric oxidants (including OH, Cl, NO₃, and O₃) to VOC groups during the observation-average (c). The contributions of different atmospheric oxidants (including OH, Cl, NO₃, and O₃) to VOC groups during the case (d). Comparisons of alkane oxidation rates (molecules·cm⁻³·s⁻¹) by OH and Cl radical during the observation-average (e). Comparisons of alkane oxidation rates by OH and Cl radical (molecules·cm⁻³·s⁻¹) during the case (f).

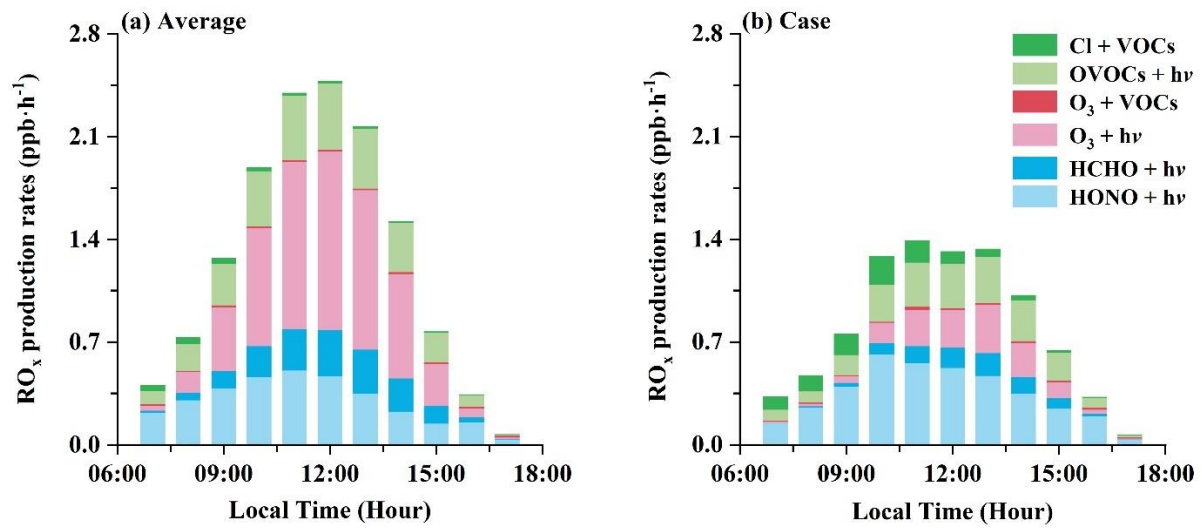


Figure 9. The contributions of different production pathways to RO_x production rates under the observation-average condition (a) and high ClNO₂ case (b), respectively.

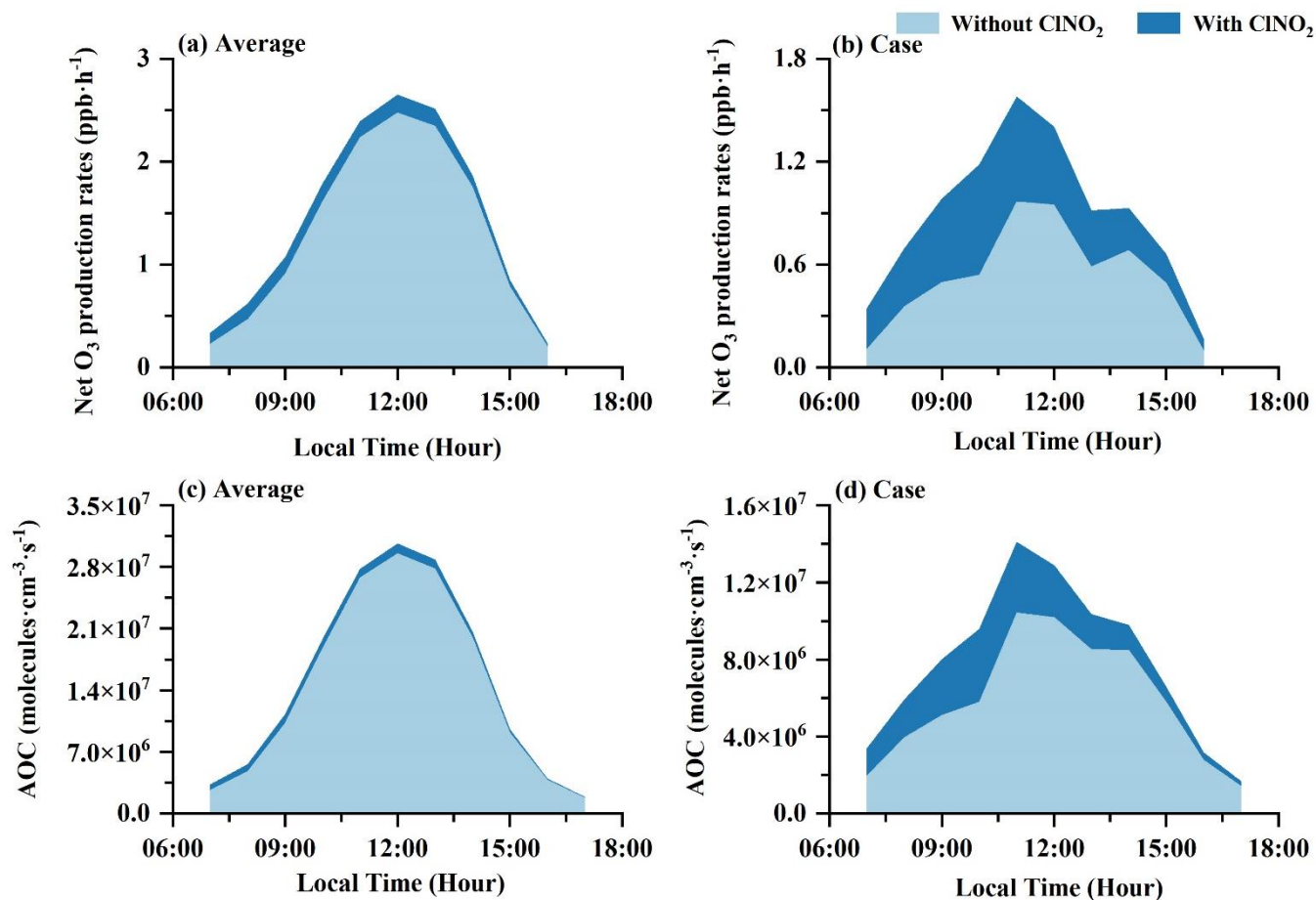


Figure 10. The impacts of Cl radicals released by ClNO₂ photolysis on net O₃ production rates and the AOC levels under the observation-average condition (a, c) and high ClNO₂ case (b, d), respectively.

Table 1. Relative importance of Cl, OH, and O₃ to the daytime oxidation of VOC groups (including alkanes, alkenes, alkynes, aromatics, and OVOCs) around the world (Xue et al., 2015; Bannan et al., 2015; Bannan et al., 2017; Rutherford et al., 1995; Fraser et al., 1997).

	Xiamen (average)	Xiamen (case)	Hong Kong (max)	London (average)	Weybourne (average)	Boston	LA
Alkane Cl%	11.7	44.8	53.0	3.5	1.0	8.5	9.9
Alkane OH%	88.3	55.2	47.0	96.5	99.0	91.5	90.1
Alkane O ₃ %	-	-	-	-	-	-	-
Alkene Cl%	12.2	8.7	14.0	0.6	0.4	0.3	0.3
Alkene OH%	85.0	75.2	81.0	77.9	78.3	33	31.3
Alkene O ₃ %	1.2	14.7	5.0	21.5	21.4	66.7	68.4
Alkyne Cl%	8.5	40.0	-	7.0	2.6	8.7	8.7
Alkyne OH%	91.5	60.0	-	91.8	96.7	89.7	89.7
Alkyne O ₃ %	-	-	-	1.2	0.7	1.6	1.6
Aromatics Cl%	0.7	9.1	11.0	-	-	-	-
Aromatics OH%	97.0	86.6	89.0	-	-	-	-
Aromatics O ₃ %	0.7	2.6	-	-	-	-	-
OVOCs Cl%	0.9	5.2	6.0	-	-	-	-
OVOCs OH%	81.4	78.7	85.0	-	-	-	-
OVOCs O ₃ %	12.0	3.9	-	-	-	-	-

Table 2. The impacts of ClNO_2 photolysis on RO_x (OH , HO_2 , and RO_2) levels, $\text{P}(\text{RO}_x)$, and $\text{P}(\text{O}_3)$ around the world (Xia et al., 2021; Wang et al., 2022; Tham et al., 2016; Wang et al., 2016; Xue et al., 2015; Bannan et al., 2017; Jeong et al., 2019).

Study Area	Season	OH	HO ₂	RO ₂	P(RO _x)	P(O ₃)
Xiamen (average)	Autumn	3.7%	7.1%	10.3%	4.9%	6.7%
Xiamen (case)	Autumn	17.9%	34.6%	54.3%	23.8%	41.7%
Wangdu/Beijing/Mt. Tai	Winter	15.0%–22.0%	24.0%–31.0%	36.0%–52.0%	1.3%–3.8%	1.3%–6.2%
Heshan	Autumn	1.5%–2.6%	1.9%–4.6%	3.0%–6.8%	< 2.2%	1.0%–4.9%
Wangdu	Summer	-	-	-	10%–30%	3.0%–13.0%
Mt. Tai Mo Shan, Hong Kong	Winter	40.0%–77.0%	53.0%–106.0%	-	-	11.0%–41.0%
Hok Tsui, Hong Kong	Summer	6.6%	12.2%	45.1%	-	10.3%
Weybourne	Spring	5.0%	7.0%	9.0%	-	-
Seoul	Spring	-	-	-	-	1.0%–2.0%

30